

Make Full Use of Testing Information: An Integrated Accelerated Testing and Evaluation Method for Autonomous Driving Systems

Xinzheng Wu^a, Junyi Chen^{a,*}, Jianfeng Wu^a, Longgao Zhang^a, Tian Xia^a and Yong Shen^a

^aSchool of Automotive Studies, Tongji University, No. 4800 Cao'an Road., Shanghai, 201804, China

ARTICLE INFO

Keywords:

Autonomous driving systems
SOTIF
Scenario-based testing
Safety evaluation
Optimization algorithm
Stopping condition

ABSTRACT

Testing and evaluation is an important step before the large-scale application of the autonomous driving systems (ADSs). Based on the three level of scenario abstraction theory, a testing can be performed within a logical scenario, followed by an evaluation stage which is inputted with the testing results of each concrete scenario generated from the logical parameter space. During the above process, abundant testing information is produced which is beneficial for comprehensive and accurate evaluations. To make full use of testing information, this paper proposes an Integrated accelerated Testing and Evaluation Method (ITEM). Based on a Monte Carlo Tree Search (MCTS) paradigm and a dual surrogates testing framework proposed in our previous work, this paper applies the intermediate information (i.e., the tree structure, including the affiliation of each historical sampled point with the subspaces and the parent-child relationship between subspaces) generated during the testing stage into the evaluation stage to achieve accurate hazardous domain identification. Moreover, to better serve this purpose, the UCB calculation method is improved to allow the search algorithm to focus more on the hazardous domain boundaries. Further, a stopping condition is constructed based on the convergence of the search algorithm. Ablation and comparative experiments are then conducted to verify the effectiveness of the improvements and the superiority of the proposed method. The experimental results show that ITEM could well identify the hazardous domains in both low- and high-dimensional cases, regardless of the shape of the hazardous domains, indicating its generality and potential for the safety evaluation of ADSs.

1. Introduction

The safety of autonomous driving systems (ADS) is a pivotal issue that demands comprehensive verification prior to the large-scale deployment (Sohrabi et al., 2021). As a crucial aspect of safety, the safety of the intended functionality (SOTIF), as defined in the automotive safety standard ISO 21448 (ISO 21448:2022), focuses on and endeavors to eliminate hazards or risks that caused by insufficiencies of specification or performance limitations of ADSs. According to the standard, in the verification phase, the SOTIF problem can be addressed by simulation testing to evaluate ADSs under known hazardous scenarios (Wang et al., 2024). Currently, based on the three level of scenario abstraction theory (Menzel et al., 2018), scenario-based simulation testing and evaluation has become the prevailing verification method to address SOTIF problem due to its low cost, high efficiency and repeatability, which has garnered widespread attention from both academia and industry (Sun et al., 2022a).

In practice, testing and evaluation are mainly conducted on the logical scenario level (Peixing Zhang, 2022). However, due to the high complexity and uncertainty of the external environment of high-level ADS, the logical scenario space constructed is usually high-dimensional, leading to the "dimensionality explosion" problem (Feng et al., 2023). To address this issue, optimization algorithms are introduced by numerous researchers to effectively search hazardous scenarios in the whole logical scenario space (Zhang et al., 2023b).

*Corresponding author

✉ chenjunyi@tongji.edu.cn (Junyi Chen)

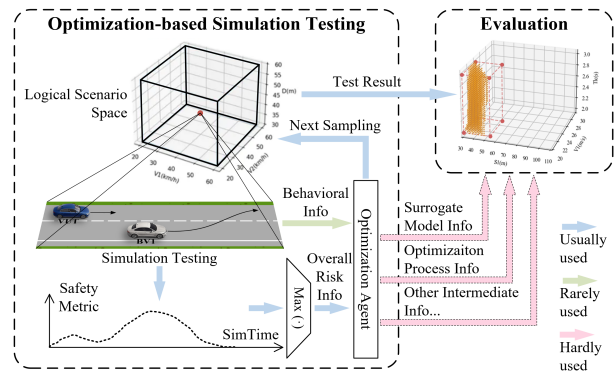


Fig. 1. Information at different layers during the testing and evaluation process.

Generally, as shown by the blue arrow in Fig. 1, during the testing process, the risk of a test scenario for the vehicle under test (VUT) is calculated simultaneously using certain safety metrics (Wang et al., 2021; Lu et al., 2021). After a test scenario is completed, an overall risk result, representing the safety performance of the VUT, can be obtained, which is then fed into the optimization agent as a cost function value. With a batch of test results obtained, the optimization agents will guide the sampling of the next batch of test scenarios towards the predicted possible hazardous areas. Finally, when the stopping condition of the optimization algorithm is satisfied, all the test results will be sent to the evaluation module for the safety verification of VUT.

Following the above technical route, existing methods have realized the accelerated generation of hazardous scenarios (Gong et al., 2023; Huang et al., 2024). However, in

the above process, only scenario risk information is used, which hinders further improvement of testing efficiency and the comprehensiveness of evaluation. In fact, all other diverse information generated during the testing process can provide insight for the testing itself as well as the evaluation. As a remedy, our previous work (Wu et al., 2024a) takes the behavioral information (as shown by the green arrow in Fig. 1) into consideration. By using a convolutional neural network (CNN) to extract the information from the trajectories of vehicles, we have constructed a dual surrogates-based accelerated testing method and improved both the efficiency and coverage of the generation of hazardous scenarios. Nevertheless, testing and evaluation remain separate in the above work. Still, only the scenario risk information is transferred to the evaluation process, ignoring the intermediate information generated during the optimization process, as shown by the pink arrow in Fig. 1. Towards addressing this issue, this paper establishes an Integrated accelerated Testing and Evaluation Method (ITEM) so as to make full use of the testing information. Compared with our previously published paper (Wu et al., 2024a), the new contributions of this paper are listed as follows:

- (1) An integrated testing and evaluation framework is proposed with the aim of leveraging testing information to obtain a more accurate and comprehensive evaluation result.
- (2) In the accelerated testing stage, the UCB calculation method is improved to enable sampling to converge at the hazardous domain boundaries, thereby facilitating accurate evaluation. Additionally, a stopping condition is constructed based on the the idea of algorithmic convergence.
- (3) In the accelerated evaluation stage, a hazardous domain identification method is proposed using both the testing results (i.e., sampling records) and the intermediate testing information (i.e., tree structure).
- (4) Two metrics, namely API and ADI, are proposed quantify the accuracy of hazardous domain identification. These two metrics are designed with considerations from the perspectives of proportional accuracy and distributional accuracy respectively.
- (5) Ablation and comparative experiments are conducted to verify the effectiveness of the improvements and the superiority of the proposed method compared with other baseline methods.

The remainder of the paper is organized as follows: Some related works and research gaps are described in Sec. 2. In Sec. 3, the framework and the improvements of ITEM is detailed. Ablation and comparative experiments are performed in Sec. 4, followed by the analysis and discussion of the experimental results. The conclusion is summarized in Sec. 5.

2. Related Works

2.1. Safety Testing Methods for Autonomous Driving Systems

In the current literature, safety testing methods for ADS can be classified as Naturalistic Driving Data-based (NDD-based), Design of Experiments-based (DOE-based), and adaptive DOE-based (ADOE-based) methods.

By statistically analyzing the collected naturalistic driving data, NDD-based methods directly extract testing scenarios to satisfy specific testing requirement. For example, by translating the data from different sources into a standardized format and calculating the possibility of recombination between scenario slices, the project PEGASUS proposed a scenario extraction and classification method (Pütz et al., 2017). Similarly, Yin et al. extracted hazardous lane-changing testing scenarios from China-FOT naturalistic data by establishing a scenario risk classification model and an excellent human driver model (Yin et al., 2023). Furthermore, Feng et al. first extracted all cut-in events in a NDD database and then applied the seed-fill method to search hazardous scenarios (Feng et al., 2020). Besides, Importance Sampling (IS) was also widely used to accelerate rare-scenario probability estimation, thus increasing the number of rare scenarios in NDD sampling (Zhao et al., 2017; Feng et al., 2021). Since the generated testing scenarios are derived from real driving data, NDD-based methods are of high realism. However, these methods rely on a large amount of high-quality data and the generated scenarios are limited to the known data, resulting in low generalizability.

Instead of directly extracting testing scenarios from the collected data, DOE-based methods design testing scenarios by using different combinations of scenario parameters, where all testing scenarios are generated before the start of the test. Combinatorial testing is a typical representative of the DOE-based approaches. Bagschik et al. constructed a five-layer scenario model and generated functional scenarios based on parameter combinations (Bagschik et al., 2018). Li et al. described the environment of VUT through an ontology model, which was then used as input for combinatorial testing (Li et al., 2020). Apart from that, methods such as random testing, near-random testing (e.g. Latin Hypercube Sampling (Batsch et al., 2019)) and grid testing can also be considered as DOE-based methods. DOE-based methods ignore the information of the VUT that is gradually acquired during the testing process, and the subsequent testing scenarios cannot be designed with reference to the test results of the completed scenarios, leading to low testing efficiency.

Compared with DOE-based methods, ADOE-based methods generate testing scenarios step by step following the idea of optimization. According to the testing results of previously generated testing scenarios, the parameters of new testing scenarios are adaptively designed to be more challenging for VUT. Currently, existing methods have applied various optimization algorithms in the safety testing

for ADS. Crespo-Rodriguez et al. utilized a single-objective genetic algorithm (GA) to search for adversarial test scenarios (Crespo-Rodriguez et al., 2024). Gladisch et al. used Systems Theoretic Process Analysis (STPA) to initiate a testing function scenario and then applied Bayesian Optimization (BO) to find hazardous combinations of test parameters and their values (Gladisch et al., 2019). Our previous work used particle swarm optimization (PSO) (Feng et al., 2022) and monte-carlo tree search (MCTS) (Wu et al., 2024b) respectively to quickly find the multimodal distributed hazardous scenarios while guaranteeing their coverage. ADOE-based methods can quickly converge on the scenarios with high testing value and have shown great potential in efficiency, coverage and stability for safety testing of ADS. Therefore, ADOE-based methods are chosen as the basis for the evaluation stage in this paper.

In ADOE-based methods, another key issue that have garnered significant scholarly attention is when the testing should stop. One category of methods intuitively defined an upper limit on number (Zhang et al., 2024) or duration (Hellwig and Beyer, 2019) that an algorithm can be run. However, with these methods based on expert experience, it is difficult to accurately set the value of the stopping condition. Another category of methods defined the stopping condition from the perspective of algorithmic convergence, e.g., by finding a predefined optimal solution (Ravber et al., 2022) or by using the convergence of a surrogate model that additionally trained using historical sampling records as the stopping criterion (Sun et al., 2022b). This type of methods can adaptively stop the sampling. However, they hold the issue of converging to local optima when there are multiple optimal solutions in ADS testing. To alleviate this effect, in this paper, we propose a more comprehensive approach to partitioning the training dataset for an observation model, whose prediction performance will be used as the stopping criterion.

2.2. Safety Evaluation Methods for Autonomous Driving Systems

With the testing results in hand, existing methods achieved safety evaluation for ADS either based on points (namely the testing results of concrete scenarios) or areas (namely hazardous domains) under a logical scenario space.

Points-based methods directly calculate the number or percentage of the hazardous concrete scenarios, in which the VUT does not fulfill the passing condition (a collision occurs or the safety metric exceeds a certain threshold), to represent the safety performance of VUT. Bussler et al. used an evolutionary algorithm to identify hazardous scenarios while the number of the identified scenarios was used to evaluate VUT (Bussler et al., 2020). Feng et al. regarded the accident rate as the evaluation metrics, where an accident was identified when the relative distance between the VUT and a virtual background vehicle was zero or less than zero under an augmented reality (AR) testing platform (Feng et al., 2020). Ding et al. proposed a flow-based multimodal

hazardous scenario generator and used collision rate as evaluation indicators (Ding et al., 2021). ISO 34502 used the ratio of passing the scenario under test as a measure of safety evaluation (ISO 34502:2022). Point-based methods can evaluate the safety level of VUT in logical scenarios to some extent, but they ignore the correlation of key parameters in the scenarios, which makes them difficult to meet the safety verification needs of high-level ADS.

Areas-based methods achieve safety evaluation by identifying hazardous domains, the number and distribution of which represent the safety performance of a VUT. Generally, hazardous domains can be obtained with classification or clustering methods. For instance, based on the sampled hazardous scenarios after testing, Mullins et al. used MeanShift, an unsupervised clustering method, to identify hazardous domains while getting their boundaries (Mullins et al., 2018). Similarly, Batsch et al. applied Gaussian Process Classification to identify the performance boundary through testing results obtained from Monte Carlo sampling and Latin Hypercube sampling (Batsch et al., 2019). Apart from the classification- and clustering-based methods, Zhang et al. introduced the gravitational field formed by the most hazardous scenarios identified during testing. By integrating this with the internal probability distribution of the logical scenario parameter space derived from naturalistic driving trajectory (NDT), the safety performance of the VUT at any point within the logical scenario could be calculated, which enabled the determination of hazardous domains (Zhang et al., 2023a). However, most of the existing literature obtained hazardous domains with irregular boundaries, which hindered further quantitative evaluation of the safety of VUT, such as identifying the exact extent and calculating the actual size of the hazardous domains, especially in high-dimensional parameter space. To circumvent this restraint, this paper uses hyper-cuboid to approximate hazardous domains to obtain regular boundaries, which enables quantitative safety evaluation.

3. Method

3.1. Framework

The framework of the proposed Integrated Accelerated Testing and Evaluation Method (ITEM) is shown in Fig. 2, which can be divided into accelerated testing stage and accelerated evaluation stage. The above two stages are integrated together to ensure that testing information is utilized as much as possible. The green parts highlight the improvements in this paper compared with our previous work (Wu et al., 2024a,b).

As depicted in Fig. 2, in the accelerated testing stage, an initial random sampling is conducted at first. After that, concrete testing scenarios are generated based on the sampling results, which are then inputted to the in-loop testing. Next, the dual surrogates model is constructed, in which both the

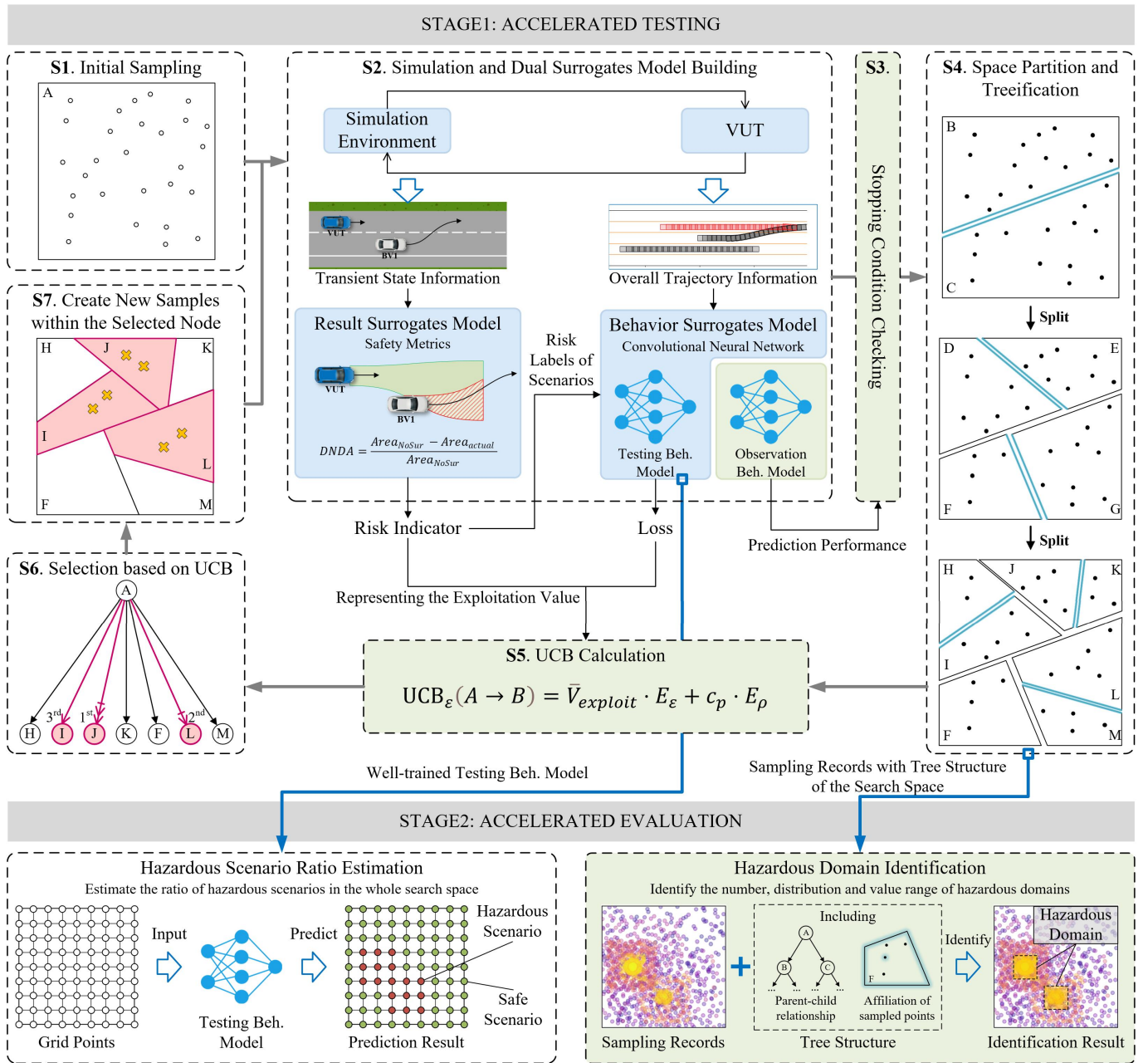


Fig. 2. Framework of the Proposed Integrated Accelerated Testing and Evaluation Method (ITEM).

transient state information during testing and the overall trajectory information after testing are utilized. More in detail, during the testing, a certain safety metric is calculated using transient state information such as positions and velocities of ego and background vehicles to construct the result surrogate model (in this paper, we apply DNDA (Wu et al., 2022) as the safety metric). And after the testing, with a bird's eye view (BEV) recording the overall trajectory information and a risk label calculated by the safety metric as input, a CNN is used to construct the behavior surrogate model. It should be noted that an additional observation behavior surrogate model is trained in this paper, whose prediction performance will be used as a reference for the stopping condition. The settings of the observation behavior surrogate model and the

construction of the stopping condition will be detailed in Sec. 3.2.2.

After checking the stopping condition, the entire logical space is recursively partitioned into good and bad subspaces based on risk values, and a tree structure is then constructed. Then, Upper Confidence Bound (UCB) of each node is calculated with the improved calculation method. Based on the UCB result, promising subspaces with a high probability of containing hazardous scenarios are chosen to generate new sampling points. The above process continues until the stopping condition is reached.

Once the accelerated testing stage is finished, the sampling records, as well as the well-trained testing behavior surrogate model and the tree structure of search space are

transferred to the accelerated evaluation stage all together, where both points-based and areas-based methods are conducted for quantitative safety evaluation. To be specific, for points-based safety evaluation method, the testing behavior surrogate model is utilized as a proxy to quickly predict and evaluate the safety performance of the VUT in concrete scenarios that have not been tested before. Through the utilization of this surrogate model, the risk levels of each scenario obtained via fine grid sampling are predicted. Consequently, an estimation of the ratio of hazardous scenarios can be derived. At the same time, for areas-based safety evaluation method, based on the parent-child relationship of each subspace stemmed from the tree structure, hazardous scenarios in the sibling subspaces can be merged into the same hazardous domain, thus achieving hazardous domain identification. Detailed information can be found in Sec. 3.3.

3.2. Improvements on Accelerated Testing Stage

Compared with our previous work (Wu et al., 2024a,b), two major improvements are proposed in this paper: 1) An improved UCB calculation method that emphasizing the value of boundary subspaces, 2) The stopping condition based on the prediction performance of an additionally trained observation model.

3.2.1. Improved UCB Calculation Method

As the basis for subspace selection, the computation result of UCB directly determines the direction and result of the searching of hazardous scenarios, and thus has been deeply investigated in our previous work. In Wu et al. (2024b), we have introduced density of subspaces into the calculation of UCB to overcome the sampling bias phenomenon. And in (Wu et al., 2024a), we have integrated UCB with the loss of CNN to choose the promising subspaces more accurately. In this paper, in order to serve the purpose of hazardous domain identification, it is necessary to find hazardous scenarios located at the boundary of the hazardous domain as many as possible. To this end, we first define boundary subspace as the subspace that contains both hazardous and safe scenarios, as shown in the following equation.

$$G = G_b, \text{ if } \max(f(\mathbf{x}_i)) > f_b \text{ and } \min(f(\mathbf{x}_i)) < f_b, \quad (1)$$

$$i \in \{1, 2, \dots, t\}$$

where G represents a subspace and G_b is the identified boundary subspace. \mathbf{x}_i is the i^{th} sampled point belonging to G that represents a concrete scenario. $f(\cdot)$ is a certain safety metric. And f_b is the threshold to determine whether the scenario \mathbf{x}_i is hazardous or not.

By attributing additional value to the identified boundary subspaces, the algorithm tends to select these boundary subspaces for searching, thereby achieving the aim of finding as many hazardous scenarios as possible at the boundary of the hazardous domains. The additional value of each

boundary subspace V_{boundary} can be calculated as:

$$V_{\text{boundary}} = \text{AVG} \left[\sqrt{\sin \left(\frac{\{\min[f(\mathbf{x}_{i,\text{above}})] - f_b\} \cdot \pi}{2(f_{\text{up}} - f_b)} \right)}, \right. \\ \left. \sqrt{\sin \left(\frac{\{f_b - \max[f(\mathbf{x}_{i,\text{below}})]\} \cdot \pi}{2(f_b - f_{\text{low}})} \right)} \right] \quad (2)$$

where f_{up} and f_{low} are the upper and lower bounds of the safety metric value. $\mathbf{x}_{i,\text{above}}$ and $\mathbf{x}_{i,\text{below}}$ represent all the points within the boundary subspace that above and below the threshold f_b . The formula first finds the closest scenarios to the threshold in $\mathbf{x}_{i,\text{above}}$ and $\mathbf{x}_{i,\text{below}}$, and then calculates the mean value of the distance of these two scenarios from the threshold to measure the degree of exploration of the hazardous domain boundary within the boundary subspace. A larger value indicates that the hazardous domain boundary is under-explored within the boundary subspace and more sampling is needed.

Additionally, in order to avoid the algorithm falling into a local optimum at the beginning due to over-sampling in the boundary subspaces, this paper introduces the idea of Random Dropout in neural network training. When the value of the boundary subspace is computed, this value is randomly deactivated with a probability P_{drop} , thus preventing over-sampling in certain boundary subspace. More in detail, the probability P_{drop} in this paper is set to an adaptive value that decreases with the increase in the number of sampled points. By doing so, it can avoid the algorithm falling into local optima in the early sampling stage, while ensuring that the algorithm focuses on the boundary subspace in the late sampling stage, which is conducive to accurately identifying the boundary of the hazardous domains. The probability P_{drop} is defines as:

$$P_{\text{drop}} = \begin{cases} 1 - 1/k \times N_{\text{sample}}, & \text{if } N_{\text{sample}} < k \\ 0, & \text{if } N_{\text{sample}} \geq k \end{cases} \quad (3)$$

where N_{sample} is the number of sampled points and k is a tunable hyperparameter, which is determined by the dimension of the search space and the sampling budget.

Finally, the UCB calculation method that considers the subspace density, the loss of the CNN, and the value of the boundary subspace is shown in Eq. 4.

$$UCB_e(A \rightarrow B) = \bar{V}_{\text{exploit}} \cdot E_e + c_p \cdot E_p \quad (4)$$

As shown in Eq. 4, the UCB from parent space A to child space B consists of two main terms. The former represents the exploitation value of subspace B , expressed as the product of the subspace value \bar{V}_{exploit} the loss E_e output by the result and behavior surrogates model on that subspace, respectively. The latter represents the exploration value of subspace B , expressed as the ratio of the density of sampled points in the parent space to the subspace (as shown in Eq. 7). c_p is a tunable hyperparameter used to balance exploitation and exploration.

Based on Eq. 4, three cases will be prioritized by the algorithm: 1) a high value $\bar{V}_{exploit}$ of the subspace, which indicates that the subspace contains numerous hazardous scenarios and is thus worthy of further exploitation, 2) a high loss E_e , which represents that the sampling in the subspace are not distinctly featured and the surrogate model is difficult to learn, and it is necessary to explore more to reduce the difficulty of learning, and 3) a high E_ρ , which represents that the subspace is not adequately explored, and it is necessary to explore more to ensure the coverage in the further search.

Further, in order to avoid a large difference between the two terms in the UCB which can lead to a failure of the balance between exploitation and exploration, it is necessary to ensure that the value domains of each term are in the same order of magnitude. In general, large values of the exploration term can cause the algorithm to converge slowly but this is acceptable to ensure coverage. However, large values of the exploitation term can cause the algorithm to fall into local optima, so it is necessary to limit the value of the exploitation term. In this paper, we first use a normalization function $N(x)$ to normalize the original values, followed by a convex function $G(x)$ to amplify the values of the nodes with low exploitation values so as to avoid falling into local optima. $N(x)$ and $G(x)$ can be expressed as:

$$N(x) = \frac{x - X_{low}}{\max(x_{all}) - X_{low}} \quad (5)$$

$$G(x) = \begin{cases} \frac{1}{1 - \log_{10}^x}, & x > 0 \\ 0, & x = 0 \end{cases} \quad (6)$$

In Eq. 5, X_{low} is the lower bound of the value domain of x . Ultimately, the terms of Eq. 4 are calculated as follows:

$$\begin{aligned} \bar{V}_{exploit} &= G[N(V_{exploit} + V_{boundary})] \\ E_e &= G[N(\bar{e}_B/\bar{e}_A)] \\ E_\rho &= \ln(\bar{\rho}_A/\bar{\rho}_B) \end{aligned} \quad (7)$$

where $V_{exploit}$ is calculated by the safety metric $f(\cdot)$ and $V_{boundary}$ is the additional value of boundary subspace. \bar{e}_A and \bar{e}_B are the average loss of the behavior surrogate model in parent node A and child node B . $\bar{\rho}_A$ and $\bar{\rho}_B$ are the average density of parent node A and child node B . The calculations of $V_{exploit}$, \bar{e}_{Node} and $\bar{\rho}_{Node}$ are essentially the same as in (Wu et al., 2024a) and (Wu et al., 2024b), but with minor modifications. The specific calculation methods of the above parameters can be found in Appendix A.

3.2.2. Stopping Condition

In this paper, we define the stopping condition based on the prediction performance of the behavior surrogate model. If the model is able to predict accurately on the test set after training with the recorded sampled points, the search is sufficiently adequate to stop, otherwise the search should be

continued. However, since all the recorded sampled points have been used to train the behavior surrogate model, there are no extra sampled points to test the prediction accuracy.

To address this issue, in addition to the testing behavior surrogate model (hereinafter called the testing beh. model) that is trained using all of the sampled points, we construct in parallel an observation behavior surrogate model (hereinafter called the observation beh. model) that is trained using only a portion of the sampled points, with the remaining sampled points being used as the test set. By doing this, we actually construct a lite version of the behavior surrogate model. Existing studies have demonstrated that the predictive performance of the model improves as the number of samples in the training set increases (Sun et al., 2017). Therefore, we can use the predictive performance of the observation beh. model to determine if the testing beh. model is adequately trained without affecting the search on the mainstream.

In order to be able to comprehensively measure the predictive performance of the observation beh. model, a representative test set covering the entire search space is required. However, since the purpose of the search is to find hazardous scenarios, the percentage of hazardous scenarios in the recorded sampled points is higher than the actual situation, so how to divide the test set is a key issue. This paper introduces the idea of spatial stratification in Latin Hypercube Sampling to form an unbiased test set. The stopping condition construction process is shown in Fig. 3.

As depicted in Fig. 3, the entire search space is first divided into equal grids (or cubes/hypercubes). After that, for each grid subspace containing historical sampled points, one of the sampled points is prioritized to be divided into the test set and the rest of the sampled points are divided into the training set. A clear example is illustrated in Fig. 3, where

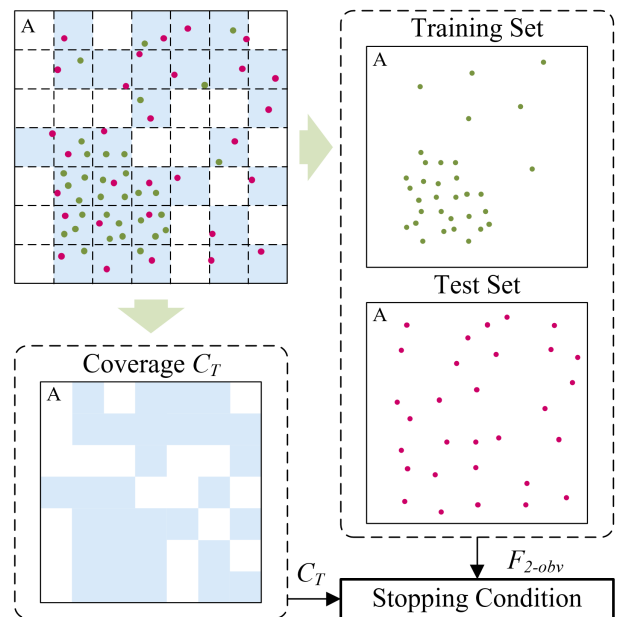


Fig. 3. The stopping condition construction process.

the test set evenly covers the entire search space. With the training set and the test set obtained, the observation behavior model is trained and then evaluated by Confusion Matrix Analysis, where we use $F_2 - Score$ (denoted as F_{2-obv}) as metric to emphasize more on Recall. Concurrently, after the search space is divided, a quantitative test set coverage metric C_T can be obtained from the ratio of the number of grids occupied by sampled points to the number of all grids. Finally, based on F_{2-obv} and C_T , the stopping condition is established: The search will stop if both of the following conditions are met:

- The test set must cover 80% of the search space ($C_T \geq 80\%$) to ensure representative test results.
- The predictive performance metric F_{2-obv} must be greater than the threshold F_s ($F_{2-obv} \geq F_s$).

3.3. Improvements on Accelerated Evaluation Stage

As illustrated in Fig. 2, both points-based and areas-based evaluation method are included in our framework. Since the points-based approach has been well described in (Wu et al., 2024a), this paper focuses on the areas-based approach to identify the hazardous domains.

Different from other studies that use only historical sampled points information, the hazardous domain identification method proposed in this paper also takes the tree structure into account. More in detail, two aspects of information are included in the tree structure transferred from the accelerated testing stage: 1) The affiliation of each historical sampled point with the subspaces, 2) The parent-child relationship between subspaces.

For ease of interpretation, a schematic diagram is demonstrated in Fig. 4, where all the subspaces are partitioned in the way shown in Fig. 2-S4, and assuming that the real distribution of the hazardous domains is as shown in the scatter plot in Fig. 2. The identification method can be divided into four steps as follows:

1) *Hazardous Scenarios Selection*: All hazardous scenarios with safety metric values $f(x_i)$ exceeding the threshold f_b are selected first, as illustrated by the yellow dots in Fig. 4. After that, only subspaces containing hazardous scenarios are retained, while non-hazardous scenarios in these subspaces are also excluded.

2) *Subspace Hazardous Domains Approximation*: Hyper-cuboids are used in this step to approximate the hazardous domain in each retained subspace, which are represented by the red boxes in Fig. 4. To be specific, the upper and lower bound of a hyper-cuboid in each dimension can be determined as:

$$\begin{cases} B_{lower,j} = \min((x)_{i,j}) \\ B_{upper,j} = \max((x)_{i,j}) \end{cases} \quad (8)$$

where $i \in \{1, 2, \dots, T\}$ represents the i^{th} hazardous scenario in a certain subspace that has totally T hazardous scenarios.

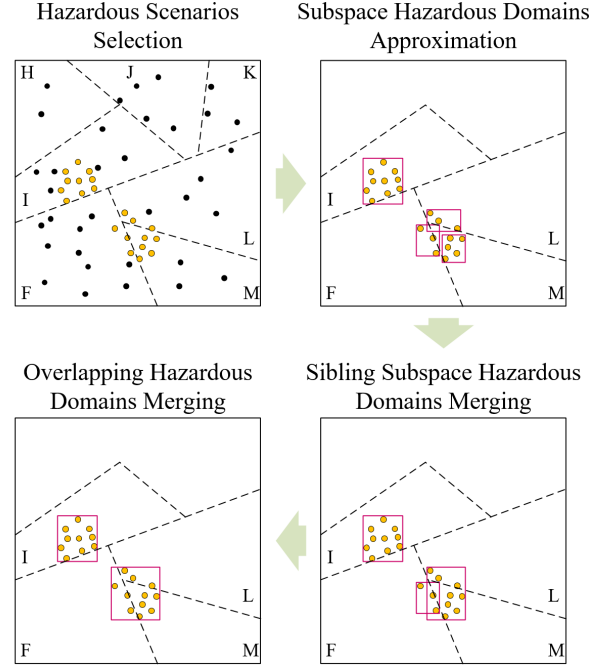


Fig. 4. Hazardous domain identification method.

$j \in \{1, 2, \dots, dim\}$ represents the j^{th} dimension that is being calculated in the dim -dimensional search space.

3) *Sibling Subspace Hazardous Domains Merging*: With the parent-child relationship between subspaces known, hazardous domains belonging to a same parent subspace are merged. As shown in Fig. 4, since both the subspace M and the subspace L are partitioned from the subspace G , they are sibling subspaces and their hazardous domains are thus merged.

4) *Overlapping Hazardous Domains Merging*: In case hazardous scenarios in the same region are identified into different hazardous domains, all the identified hazardous domains will be checked if they overlap with other hazardous domains and then merged. Note that only two hazardous domains overlapping in all dimensions will be merged. In Fig.4, the hazardous domains in subspace F and G (parent subspace of L and M) are merged because they overlap in all two dimensions, while the hazardous domain in subspace I remains independent because it does not overlap with the merged hazardous domain. Finally, two hazardous domains are identified with their shapes represented by two rectangles.

4. Experiments

4.1. Synthetic Function and Practical Scenario for Testing

In this paper, both synthetic function and practical scenario are considered. Meanwhile, the experiments cover cases from two to four dimensions, demonstrating the effectiveness of the method under both low and high dimensions.

4.1.1. Two- and Four-dimensional Multimodal Gaussian Function

This paper modifies the gaussian function, which only has one global optimum (i.e., one modality), into a multimodal gaussian function that can be defined as follows:

$$f(\mathbf{x}) = \sum_{i=1}^{dim} e^{-\frac{x_i^2}{2\sigma^2}}, \text{ where } x_i = \|\mathbf{x} + M_{(i,:)}\|_2, \quad (9)$$

for all $i = 1, 2, \dots, dim$

in which,

$$M = \begin{bmatrix} 1 & 0 & \dots & 0 \\ 0 & 1 & \dots & 0 \\ \vdots & \vdots & \ddots & \vdots \\ 0 & 0 & \dots & 1 \end{bmatrix}_{dim} \times bias \quad (10)$$

where $\mathbf{x} = (x_1, x_2, \dots, x_{dim})$ represents a certain point in the search space. dim is the dimension assigned to the function. $M_{(i,:)}$ represents the i^{th} row of the matrix M . $bias$ and σ are hyperparameters that determine the size and distribution of the hazardous domains of the function. Based on Eq. 9, the multimodal gaussian function with dim dimensions has dim modalities, which are respectively located in $x_1^* = (-bias, 0, \dots, 0)$, $x_2^* = (0, -bias, \dots, 0)$, \dots , $x_{dim}^* = (0, 0, \dots, -bias)$.

Specifically in this paper, the search space is built with a range of $x_i \in [-20, 20]$ in each dimension, and the value domains of both functions are $[0, 1]$. The hazardous threshold f_b is chosen as 0.8 (i.e., points with a function value greater than 0.8 will be considered hazardous). Moreover, hyperparameters are set as $bias = 10$ and $\sigma = 3$ in both functions. For the two-dimensional function, an illustration is given in Fig. 5, with red lines representing f_b . It can be seen that two modalities are located in $(0, -10)$ and $(-10, 0)$ as expected. As for the four-dimensional function, by numerical calculation, it can be estimated that the percentage of the

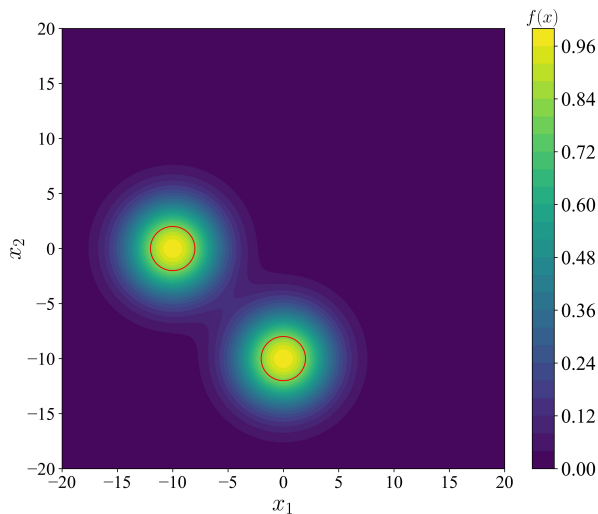


Fig. 5. Illustration of 2-dimensional multi-modal Gaussian function.

hazardous domains in the whole search space is 4.15×10^{-5} , which is consistent with the sparse distribution of hazardous scenarios in the real world, and at the same time challenging enough as a test function.

4.1.2. Three-dimensional Cut-in Scenario

Based on the simulation platform Virtual Test Drive (VTD) (Hexagon, 2025), a logical testing scenario is conducted. As demonstrated in Fig. 6, the VUT, which is controlled by the built-in ADS in VTD, is driving in the left lane with an initial speed of V_0 , ahead of which a background vehicle BV1 is driving in the middle lane at a distance S_1 . At t seconds after the start of the test, BV1 will perform a cut-in maneuver at the speed of V_1 , and the whole cut-in process will last for T_{lc} seconds. Detailed parameters of this logical testing scenario can be found in Table 1, where S_1 , V_1 and T_{lc} are parameters that construct the 3-dimensional search space, while V_0 and t are fixed parameters. Additionally, we choose DNDA (Wu et al., 2022) as the safety metric. DNDA is a normalized risk indicator based on drivable area. The closer its value is to 1, the more hazardous the scenario is. And a collision occurs when its value is equal to 1.

Unlike synthetic functions where the distribution of hazardous points can be quickly obtained through numerical computation, the distribution of hazardous scenarios in the logical scenario space needs to be obtained through simulation. To this end, a $30 \times 30 \times 30$ grid testing is executed to obtain the ground truth distribution of hazardous scenarios, which can be used as a reference for subsequent evaluation. In this experiment, scenarios with a maximum DNDA value of more than 0.8 are considered hazardous. For ease of

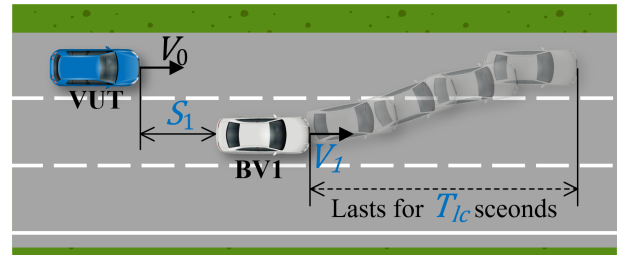


Fig. 6. Three-dimensional logical testing scenario.

Table 1
Parameter Settings of the Logical Testing Scenario.

Parameter	Denotation	Value/Range	Unit
Initial velocity of VUT	V_0	30	m/s
Initial distance between VUT and BV1	S_1	[30, 110]	m
Initial velocity of BV1	V_2	[20, 30]	m/s
Duration of lane change for BV1	T_{lc}	[2, 3]	s
Starting moment of lane change for BV1	t	3	s

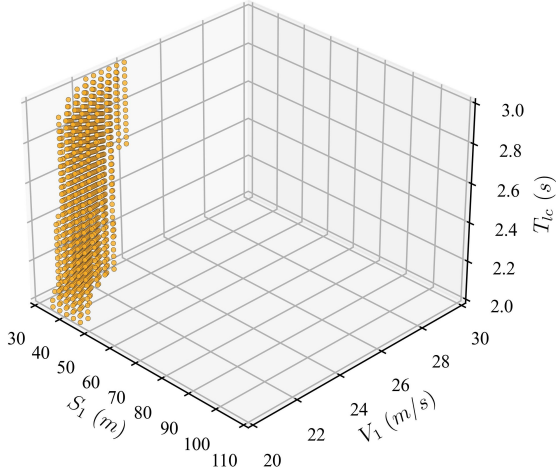


Fig. 7. Hazardous scenarios distribution in the logical testing scenario.

visualization, Fig. 7 only shows the hazardous scenarios.

4.2. Algorithms to be Tested

To validate the effectiveness of the improved method proposed in this paper as well as its superiority compared to other baseline methods, both the ablation experiment and the comparative experiment are conducted. The tested algorithms are detailed as follows.

1) *Integrated accelerated Testing and Evaluation Method (ITEM)* : ITEM is the method proposed in this paper, which uses the improved UCB considering the value of boundary subspaces as described in Sec. 3.2.1 and makes full use of the testing information in the evaluation stage.

2) *Integrated accelerated Testing and Evaluation Method with the Original UCB (ITEMoriUCB)* : Compared with ITEM, ITEM with the original UCB uses the original UCB calculation method in Wu et al. (2024a) , which doesn't take the boundary value into account.

3) *Gaussian Distribution Method with Optimization Sampling (GDMos)* : GDM is an evaluation method proposed in Zhu et al. (2022), which uses gaussian distribution to cluster the hazardous scenarios and then obtains the hazardous domains. GDM is originally input with sampled points obtained by the optimization search method in Zhu et al. (2022). Since this evaluation method is independent of the testing stage, for the fairness of the comparison, this paper uses the sampling results of ITEM in the accelerated testing stage as the input to GDM.

4) *Gaussian Distribution Method with Random Sampling (GDMrs)* : To further investigate the impact of different search algorithms in the testing stage on the evaluation stage, this paper also conducts random sampling and inputs the sampling results into the GDM.

Detailed information of each algorithm is listed in Table 2. It should be noted that the input to the behavior surrogate model must be scenario trajectory information. Consequently, neither the behavior surrogate model nor the

Table 2

Experimental Settings of the Algorithms.

Test case	Algorithm	UCB Selection	Surrogate Model	Sampling Budget
2-d function	ITEM	Improved	Single (only res)	900
	ITEMoriUCB	Original		
	GDMos	Improved		
	GDMrs	\		
3-d scenario	ITEM	Improved	Dual (res+beh)	Depend on the stopping condition
	ITEMoriUCB	Original		
	GDMos	Improved		
	GDMrs	\		
4-d function	ITEM	Improved	Single (only res)	30000
	ITEMoriUCB	Original		
	GDMos	Improved		
	GDMrs	\		

* res: result surrogate model, beh: behavior surrogate model

stopping condition is available on the two synthetic functions. Thus, for the 2- and 4-d multimodal gaussian functions, this paper only applies the result surrogate model in the accelerated testing stage and uses a predefined sampling budget as the stopping condition.

4.3. Evaluation Metrics

The main purpose of this paper is to make full use of the intermediate testing information into the safety evaluation, thus focusing more on the effect of improvements on the evaluation stage. Therefore, this paper proposes two indicators to quantify the evaluation performance, namely the accuracy of hazardous domain distribution identification (ADI) and the accuracy of hazardous domain percentage identification (API). For the evaluation metrics in the testing stage, this paper follows the $F_2 - Score$ mentioned in Wu et al. (2024b) (denoted as F_{2-grid} in this paper).

1) F_{2-grid} : $F_2 - Score$ is a typical evaluation metric that widely used in machine learning. Compared with F_{2-obv} which uses the test set divided from the sampling records as the actual values in confusion matrix, F_{2-grid} uses the grid testing data in Fig. 7 to see if the algorithm correctly predicts the values at the grid points. Noted that calculating F_{2-grid} takes more computational resources than calculating F_{2-obv} because the predicted values for all grid points need to be calculated. Therefore, F_{2-grid} is only used for the evaluation of different algorithms and not for the determination of the stopping conditions.

2) *Accuracy of Hazardous Domain Percentage Identification (API)* : API is used to measure the percentage of ground truth hazardous domains covered by identified hazardous domains. Suppose there are n hazardous domains in the dim -dimensional search space A , and the range of

each ground truth hazardous domain HD_{GT}^i in each dimension is $[a_d^i, b_d^i]$, where $i = 1, 2, \dots, n$, $d = 1, 2, \dots, dim$. Meanwhile, after the evaluation stage, totally m hazardous domains HD_{ID}^j are identified with the range $[p_d^j, q_d^j]$ on each dimension, where $j = 1, 2, \dots, m$, $d = 1, 2, \dots, dim$. Then API can be calculated as:

$$API = \frac{1}{2n} \sum_{i=1}^n \left(\frac{V_{Overlap}^i}{V_{GT}^i} + \frac{V_{Overlap}^i}{V_{ID}^{sum \sim i}} \right) \quad (11)$$

where $V_{Overlap}^i$ represents the (hyper)volume of overlap of all identified hazardous domains with the i^{th} ground truth hazardous domain, whose (hyper)volume is V_{GT}^i . $V_{ID}^{sum \sim i}$ is the sum of the (hyper)volumes of all identified hazardous domains that overlap with HD_{GT}^i . Algorithm 1 shows the calculation method of $V_{Overlap}^i$.

3) *Accuracy of Hazardous Domain Distribution Identification (ADI)*: ADI is used to quantify the extent to which the spatial distribution of identified hazardous domains differs from the ground truth hazardous domains. Using the same notations, the distance between the centroids of two hazardous domains, HD_{GT}^* and HD_{ID}^* , which are determined as overlapping in accordance with Algorithm 1, can be computed via Equation 12.

$$D_{center}^j = \sqrt{\sum_{d=1}^{dim} \left[\frac{(a_d^i + b_d^i) - (p_d^j + q_d^j)}{2} \right]^2} \Bigg|_{i=*, j=*} \quad (12)$$

Then the ADI of HD_{ID}^* can be obtained.

Algorithm 1 Calculation Method of $V_{Overlap}^i$

Input:

- $[a_d^i, b_d^i]$, Upper and lower boundaries of i^{th} ground truth hazardous domains in each dimension;
- $[p_d^j, q_d^j]$, Upper and lower boundaries of j^{th} identified hazardous domains in each dimension;
- m , Number of identified hazardous domains;
- dim , Dimension of the search space.

Output:

- $V_{Overlap}^i$, Overlapping volume.
 - 1: Volume $\leftarrow 0$
 - 2: **for** $j = 1$ to m **do**
 - 3: V $\leftarrow 0$
 - 4: **for** $d = 1$ to dim **do**
 - 5: Begin $\leftarrow \max(a_d^i, p_d^j)$
 - 6: End $\leftarrow \min(b_d^i, q_d^j)$
 - 7: Len $\leftarrow \max(0, \text{End} - \text{Begin})$
 - 8: V $\leftarrow V \times \text{Len}$
 - 9: **end for**
 - 10: Volume = Volume + V
 - 11: **end for**
 - 12: **return** Volume
-

$$ADI_j = 1 - \frac{D_{center}^j}{D_{max}^i} \Bigg|_{i=*, j=*} \quad (13)$$

where D_{max}^i is the distance from the centroid of HD_{GT}^* to a certain vertex. Finally, the ADI of all the identified hazardous domains are calculated as shown in Eq. 14.

$$ADI = \frac{1}{n} \sum_{i=1}^n \frac{1}{l} \sum_{j=x}^{x+l} ADI_j \quad (14)$$

Considering the case that a same ground truth hazardous domain may be identified as multiple hazardous domains, Eq. 14 first calculates the average of the ADI_j for a total of l identified hazardous domains that all overlap with HD_{GT}^i , and then calculate the final ADI.

4.4. Results and Analysis

The results of the evaluation metrics for each algorithm are shown in the Table 3. All the evaluation metrics are calculated after the sampling budgets are run out. In the 3-d cut-in scenario experiment, the search is stopped at 2750 samples according to the stopping condition, which is detailed in Sec. 4.5.

4.4.1. The Efficiency of the Proposed ITEM

As shown in Table 3, ITEM achieves the best performance compared with other baseline methods on both API and ADI metrics, showing the effectiveness and superiority of the proposed method in this paper.

Compared to ITEMoriUCB that uses the original UCB calculation method, ITEM obtains higher API and ADI in the evaluation stage, as well as an approximately equal F_{2-grid} in the testing stage, indicating that ITEM enhances the evaluation performance without affecting the testing efficiency. This part will be detailed in Sec. 4.4.2. Compared to GDMos which uses the same sampling records from the testing stage, ITEM outperforms it by 20%, 28.5% and 10.6% respectively for the three cases in terms of API, indicating that the identified hazardous domains of ITEM cover more of the ground truth hazardous domains and have fewer overestimations.

When it comes to the performance of ITEM on different test cases, it can be seen that in the two low-dimensional cases, both API and ADI of ITEM exceed 0.9, representing an accurate identification of the percentage and distribution of hazardous domains. While in the 4-dimensional case, ITEM obtains a high ADI of 0.980 but a relatively low API. By analyzing the detailed boundary data, we find that the identified hazardous domains achieve essentially more than 90% coverage in each dimension of each modality, but since the hypervolume calculation in Eq. 11 is multiplicative, the volume ratio will inevitably decrease as the dimensions get higher. Therefore, a slightly lower API is acceptable for high-dimensional cases.

Table 3
Results of the Evaluation Metrics for Each Algorithm.

Algorithm	2-d function			3-d scenario			4-d function		
	F_{2-grid}	API	ADI	F_{2-grid}	API	ADI	F_{2-grid}	API	ADI
ITEM (ours)	0.985	0.965	0.993	0.947	0.911	0.911	0.962	0.845	0.980
ITEMoriUCB	0.990	0.950	0.973	0.953	0.876	0.778	0.952	0.840	0.973
GDMos	0.985	0.765	0.966	0.947	0.626	0.593	0.962	0.739	0.934
GDMrs	0.829	0.719	0.938	0.855	0.629	0.642	0.029	NaN	NaN

4.4.2. The Efficiency of the Improved UCB

As discussed above, the use of the improved UCB does not diminish the efficiency of the algorithm in the testing stage (in some cases the search efficiency is even higher), while it significantly improves the accuracy of the hazardous domain identification in the evaluation stage. An illustration of the sampling dynamics of ITEMoriUCB and ITEM on the 2-d test case is shown in Fig. 8. For the entire search space, both algorithms converge quickly to the two hazardous domains of the synthetic function after only a small amount of global sampling. However, when we concentrate on a certain modality, a clear difference between the two algorithms is observed. As shown in the magnified parts of Fig. 8, ITEMoriUCB focuses only on the most hazardous regions and continues sampling on the center of the modality, whereas ITEM places more samples in the vicinity of the boundary of the hazardous domain, resulting in a full exploration of the hazardous domain boundary.

Note that even though there is a large difference between the two algorithms in the visualization results of the 2-d case, this difference is not obviously reflected in the computed API and ADI. We speculate that this is because the ground truth hazardous domains are circles, and even if ITEMoriUCB only focuses on sampling at modality centers, there will still be sporadic sampled points falling near the boundary of the hazardous domains, which improves the accuracy of hazardous domain identification. This phenomenon does not occur in the 3-d case, since its ground truth hazardous points show a rectangular distribution.

4.4.3. The Impact of the Shape of the Ground Truth Hazardous Domains

From the above analysis, we can find that the shape of the ground truth hazardous domain has a significant effect on the accuracy of hazardous domain identification. Furthermore, it can be found from Table 3 that all the algorithms get a higher value of ADI on both synthetic functions, whereas the ADI results are lower in the cut-in scenario, except for ITEM. We argue that this is because the ground truth hazardous points are isotropically distributed in both synthetic functions, so that even if the sampling is focused only on the modality center, it can still guarantee the accuracy of the distribution

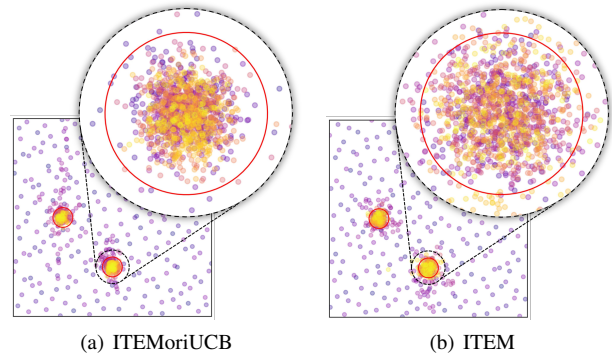


Fig. 8. Illustration of the sampling dynamics. Color from purple to golden represents the record being sampled at the beginning to the end of the optimization.

identification. As a comparison, since the ground truth hazardous points in the 3-d case are anisotropically distributed, all the baseline algorithms focusing only on the center of modalities do not have a high ADI in this case, while the method proposed in this paper still obtains an ADI of more than 0.9.

In practice, in some relative studies (Sun et al., 2022b; Zhu et al., 2022) and standards such as UN ECE R157 (UN ECE R157), the distribution of the hazardous scenarios are always anisotropic and the ground truth hazardous domains vary in shape. Therefore, an algorithm that is independent of the shape of hazardous domains is needed to achieve accurate identification of hazardous domains in various scenarios. The results in Table 3 show that the ITEM proposed in this paper is highly versatile and has great potential for hazardous domain identification in diverse logical scenarios.

4.4.4. The Impact of Search Algorithms on the Evaluation Stage

For GDM, in our experiment we respectively use the sampled points obtained from the optimization search and the random search as inputs for hazardous domains identification. From Table 3, it can be found that the identification results obtained based on the optimization sampled points are better than those obtained based on the randomly sampled points. And this gap is particularly noticeable in the 4-d case, where the F_{2-grid} of GDMrs is only 0.029

because of the high dimensionality and the sparse distribution of hazardous points, resulting in almost no hazardous points available for hazardous domain identification. The above discussion illustrates that sampling efficiency in the testing stage has a significant impact on the evaluation stage, especially in a high-dimensional search space. Since the efficiency and coverage of the optimization algorithm used in our method have been well validated in Wu et al. (2024b), ITEM can be provided with a comprehensive input in the evaluation stage to ensure an accurate identification of the hazardous domains.

4.4.5. Analysis of the Application of the Identified Hazardous Domains

Based on experimental results of the 3-d cut-in scenario, this section delves into the real-world implications of an identified hazardous domain within a practical context. Moreover, this section conducts a further examination of how the results of hazardous domain identification can be applied to safety evaluation. The testing and evaluation results of ITEM on the 3-d cut-in scenario is shown in Fig. 9, where the yellow dots represent the searched hazardous scenarios (these scenarios have a DNDA > 0.8), while the green dots represent the searched safe scenarios. The red dashed rectangular box in Fig. 9 is the hazardous domain identified by ITEM.

As shown in Fig. 9, it is evident that the points searched by the algorithm are distinctly clustered within and in the vicinity of the hazardous area as shown in Fig. 7, demonstrating the algorithm's capacity to accelerate the testing process. Secondly, all the searched hazardous scenarios are identified as one hazardous domain. In order to analyze the similarities and differences of different hazardous scenarios within the same hazardous domain, we select the two most distant hazardous scenarios within the hazardous domain (namely the Hazardous scenario 1 and 2 labeled in Fig. 9) for a case study. The two scenarios are visualized in Fig. 10,

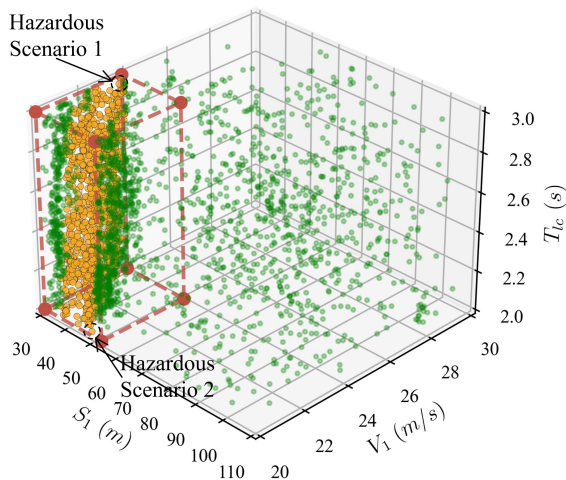
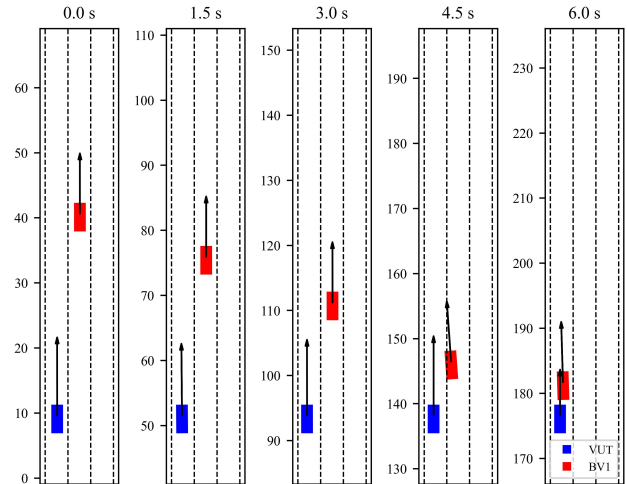


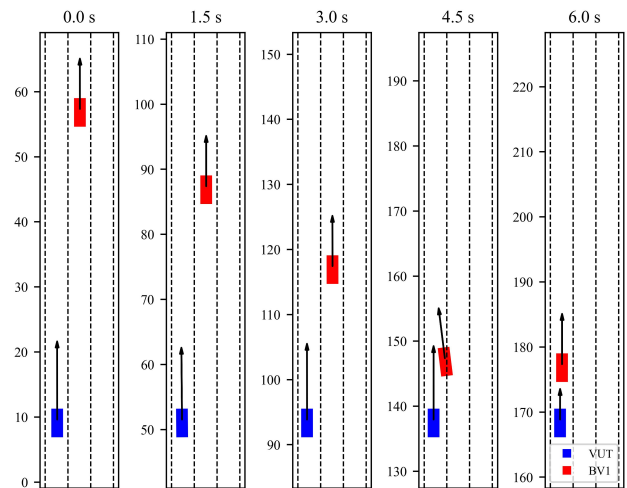
Fig. 9. Testing and evaluation results of ITEM on the 3-d cut-in scenario.

with the length of the arrow representing the velocity of the vehicles.

By observing Fig. 10, we can find that although the initial conditions are different in the two scenarios, the hazards occur for the same reason. Specifically, in both scenarios, BV1 starts to change lanes at 3s, and then at 4.5s, BV1 starts to/has entered the VUT's lane. However, at this moment, VUT does not execute any evasive maneuvers and remains in its original speed. Actually, it is not until BV1 almost completes its lane changing maneuver that VUT begins to brake. The delayed response of the VUT is inferred to be the cause of the hazards in both scenarios. The above analysis leads us to the conclusion: Different hazardous scenarios within the same hazardous domain share the same hazard generation mechanism. Therefore, when evaluating the safety performance of VUTs, it is sufficient to analyze only one scenario in each hazardous domain, rather than analyzing each hazardous scenario individually, which significantly enhances the efficiency of safety evaluation.



(a) Hazardous Scenario 1. ($S_1 = 31.48m$, $V_1 = 23.53m/s$, $T_{tc} = 2.96s$)



(b) Hazardous Scenario 2. ($S_1 = 48.72m$, $V_1 = 20.03m/s$, $T_{tc} = 2.02s$)

Fig. 10. Visualization of the two selected hazardous scenarios.

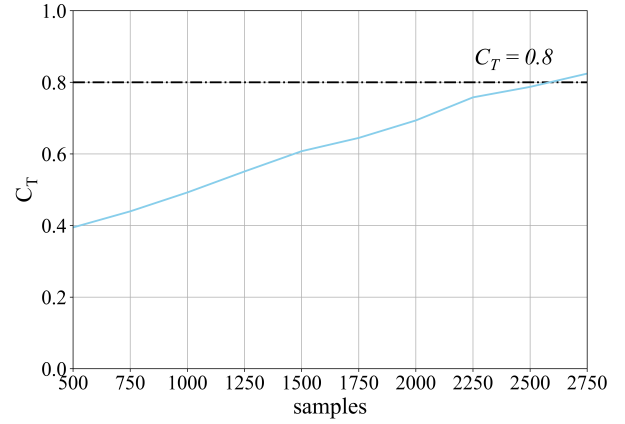
4.5. Stopping Condition Validation

The stopping condition proposed in this paper is used in the 3-d cut-in scenario. Specifically, we perform the stopping condition checking after 500 samples because the initial sampling is sparse. Then the stopping condition is checked every 250 samples. During the above process, the two stopping indicators C_T and F_{2-obv} are examined in each round to determine whether the search should stop or not. Their trend with the number of samples is shown in Fig. 11. Furthermore, the F_{2-grid} is also given as a reference to verify that the search algorithm stops at the correct time.

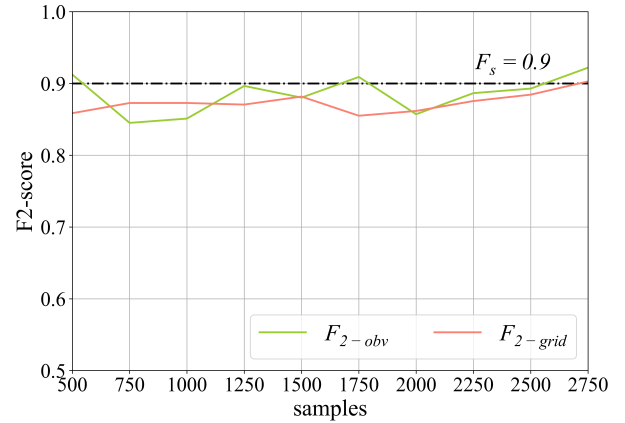
As shown in Fig. 11, the threshold F_s is chosen as 0.9 in this experiment. When the search proceeds to 2750 samples, both C_T and F_{2-obv} satisfy the stopping requirements and the search stops. At this moment, F_{2-grid} exactly reaches 0.9. Therefore, the stopping condition proposed in this paper ensures the adequacy of the search without wasting additional computational resources. Additionally, it can be seen in Fig. 11 that F_{2-obv} exceeds 0.9 several times before the search algorithm finally stops. However, at those points, F_{2-grid} still maintains a low value, indicating an inadequate search and the stopping condition is not triggered due to the low C_T , which shows again the reasonableness of the stopping condition setting in this paper.

5. Conclusion

This paper proposes an integrated accelerated testing and evaluation method (ITEM) for ADSs with the goal to make full use of the testing information. Based on a Monte Carlo tree search paradigm and a dual surrogates testing framework proposed in our previous work, this paper considers the testing stage and the evaluation stage as a whole and bridges the gap between the two stages. Specifically, to serve the purpose of accurate hazardous domains identification in the evaluation stage, we first modify the UCB calculation method to focus more on the boundary subspaces that contain both hazardous and safe scenarios. By doing this the hazardous boundaries are carefully explored. Next, we propose a hazardous domain identification method using both the sampled points and the tree structure (which contains information of the affiliation of each historical sampled point with the subspaces and the parent-child relationship between subspaces) to obtain rectangular hazardous domains. After that, to validate the proposed method, we propose two evaluation metrics (namely, API and ADI) to calculate the accuracy of the proportional and distributional identification. Experimental results show that our method outperforms other baseline methods in terms of accuracy and generality. And the efficiency of the improvements is also verified through ablation experiments. Additionally, we construct a stopping condition based on the convergence of the optimization algorithm to enable self-stopping of the testing so that the computational resources will not be wasted.



(a) The stopping condition coverage indicator C_T



(b) The stopping condition predictive performance indicator F_{2-obv} , with F_{2-grid} as a reference

Fig. 11. Stopping Condition Validation.

Since both hazardous scenario ratio estimation and hazardous domain identification are included in our framework, our future work will focus on the hazardous scenario ratio computation within each identified hazardous domain, which will lead to a more precise and comprehensive evaluation of the safety performance of ADSs. At the same time, more advanced ADSs in higher dimensional scenarios will be carried out to demonstrate the practical value of our proposed method.

A. Appendix

The calculations of $V_{exploit}$, \bar{e}_{Node} and $\bar{\rho}_{Node}$ are essentially the same as in Wu et al. (2024a) and Wu et al. (2024b) with minor modifications. For ease of understanding, here we give a summary of the calculation formulas for all these parameters.

The exploitation value of the child node B $V_{exploit}$ is calculated as:

$$V_{exploit} = \sum_{\mathbf{x} \in D_B} f(\mathbf{x}) w_B(\mathbf{x}) \quad (15)$$

In which,

$$w_B(\mathbf{x}) = \frac{1/\rho(\mathbf{x})}{\sum_{\mathbf{x} \in D_B} 1/\rho(\mathbf{x})} \quad (16)$$

where D_B is the set of all sampled points in node B . $f(\mathbf{x})$ is the risk result calculated by the safety metric. $w_B(\mathbf{x})$ is the density weight of the sampled point \mathbf{x} . $\rho(\mathbf{x})$ is the density at \mathbf{x} , which is estimated by Kernel Density Estimator (KDE).

With the density weight of each sampled point known, the average density $\bar{\rho}_{Node}$ and average loss \bar{e}_{Node} of a certain node can be obtained by Eq. 17.

$$\begin{aligned} \bar{\rho}_{Node} &= \sum_{\mathbf{x} \in D_B} w_{Node}(\mathbf{x})\rho(\mathbf{x}) \\ \bar{e}_{Node} &= \sum_{\mathbf{x} \in D_B} w_{Node}(\mathbf{x})e(\mathbf{x}) \end{aligned} \quad (17)$$

where $e(\mathbf{x})$ is the loss function of the behavior surrogate model.

CRedit authorship contribution statement

Xinzheng Wu: Formal analysis, Methodology, Software, Visualization, Writing - original draft. **Junyi Chen:** Formal analysis, Project administration, Validation, Writing - review & editing. **Jianfeng Wu:** Conceptualization, Formal analysis, Writing - review & editing. **Longgao Zhang:** Data curation, Software, Validation. **Tian Xia:** Investigation, Data curation, Validation. **Yong Shen:** Investigation, Resources, Supervision.

References

- Bagschik, G., Menzel, T., Maurer, M., 2018. Ontology based scene creation for the development of automated vehicles, in: 2018 IEEE Intelligent Vehicles Symposium (IV), pp. 1813–1820. doi:10.1109/IVS.2018.8500632.
- Batsch, F., Daneshkhan, A., Cheah, M., Kanarachos, S., Baxendale, A., 2019. Performance boundary identification for the evaluation of automated vehicles using gaussian process classification, in: 2019 IEEE Intelligent Transportation Systems Conference (ITSC), pp. 419–424. doi:10.1109/ITSC.2019.8917119.
- Bussler, A., Hartjen, L., Philipp, R., Schuldt, F., 2020. Application of evolutionary algorithms and criticality metrics for the verification and validation of automated driving systems at urban intersections, in: 2020 IEEE Intelligent Vehicles Symposium (IV), pp. 128–135. doi:10.1109/IV47402.2020.9304662.
- Crespo-Rodriguez, V., Neelofar, Aleti, A., 2024. Pafot: A position-based approach for finding optimal tests of autonomous vehicles. arXiv:2405.03326.
- Ding, W., Chen, B., Li, B., Eun, K.J., Zhao, D., 2021. Multimodal safety-critical scenarios generation for decision-making algorithms evaluation. IEEE Robotics and Automation Letters 6, 1551–1558. doi:10.1109/LRA.2021.3058873.
- Feng, S., Feng, Y., Yan, X., Shen, S., Xu, S., Liu, H.X., 2020. Safety assessment of highly automated driving systems in test tracks: A new framework. Accident Analysis & Prevention 144, 105664. doi:10.1016/j.aap.2020.105664.
- Feng, S., Feng, Y., Yu, C., Zhang, Y., Liu, H.X., 2021. Testing scenario library generation for connected and automated vehicles, part i: Methodology. IEEE Transactions on Intelligent Transportation Systems 22, 1573–1582. doi:10.1109/TITS.2020.2972211.
- Feng, S., Sun, H., Yan, X., Zhu, H., Zou, Z., Shen, S., Liu, H.X., 2023. Dense reinforcement learning for safety validation of autonomous vehicles. Nature 615, 620–627. doi:10.1038/s41586-023-05732-2.
- Feng, T., Liu, L., Xing, X., Chen, J., 2022. Multimodal critical-scenarios search method for test of autonomous vehicles. Journal of Intelligent and Connected Vehicles 5, 167–176. doi:10.1108/JICV-04-2022-0016.
- Gladisch, C., Heinz, T., Heinzemann, C., Oehlerking, J., von Vietinghoff, A., Pfitzer, T., 2019. Experience paper: Search-based testing in automated driving control applications, in: 2019 34th IEEE/ACM International Conference on Automated Software Engineering (ASE), pp. 26–37. doi:10.1109/ASE.2019.00013.
- Gong, X., Feng, S., Pan, Y., 2023. An adaptive multi-fidelity sampling framework for safety analysis of connected and automated vehicles. IEEE Transactions on Intelligent Transportation Systems 24, 14393–14405. doi:10.1109/TITS.2023.3296716.
- Hellwig, M., Beyer, H.G., 2019. Benchmarking evolutionary algorithms for single objective real-valued constrained optimization – a critical review. Swarm and Evolutionary Computation 44, 927–944. doi:10.1016/j.swevo.2018.10.002.
- Hexagon, 2025. Virtual test drive: Complete tool-chain for driving simulation applications. <https://www.mscsoftware.com/product/virtual-test-drive>.
- Huang, Y., Sun, J., Tian, Y., 2024. A bayesian optimization method for finding the worst-case scenarios of autonomous vehicles. IEEE Transactions on Intelligent Transportation Systems , 1–15doi:10.1109/TITS.2024.3490616.
- ISO 21448:2022, 2022. ISO 21448: Road Vehicles-Safety of the Intended Functionality. Standard. International Organization for Standardization. Geneva, CH.
- ISO 34502:2022, 2022. ISO 34502: Road vehicles — Test scenarios for automated driving systems — Scenario based safety evaluation framework. Standard. International Organization for Standardization.
- Li, Y., Tao, J., Wotawa, F., 2020. Ontology-based test generation for automated and autonomous driving functions. Inf. Softw. Technol. 117. doi:10.1016/j.infsof.2019.106200.
- Lu, C., He, X., van Lint, H., Tu, H., Happee, R., Wang, M., 2021. Performance evaluation of surrogate measures of safety with naturalistic driving data. Accident Analysis & Prevention 162, 106403. doi:10.1016/j.aap.2021.106403.
- Menzel, T., Bagschik, G., Maurer, M., 2018. Scenarios for development, test and validation of automated vehicles, in: 2018 IEEE Intelligent Vehicles Symposium (IV), pp. 1821–1827. doi:10.1109/IVS.2018.8500406.
- Mullins, G.E., Stankiewicz, P.G., Hawthorne, R.C., Gupta, S.K., 2018. Adaptive generation of challenging scenarios for testing and evaluation of autonomous vehicles. Journal of Systems and Software 137, 197–215. doi:10.1016/j.jss.2017.10.031.
- Peixing Zhang, B.Z., 2022. Performance evaluation method for automated driving system in logical scenario. Automotive Innovation 5, 299–310. doi:10.1007/s42154-022-00191-3.
- Pütz, A., Zlocki, A., Küfen, J., Bock, J., Eckstein, L., 2017. Database approach for the sign-off process of highly automated vehicles, in: 25th International Technical Conference on the Enhanced Safety of Vehicles (ESV).
- Ravber, M., Liu, S.H., Mernik, M., Črepinšek, M., 2022. Maximum number of generations as a stopping criterion considered harmful. Applied Soft Computing 128, 109478. doi:10.1016/j.asoc.2022.109478.
- Sohrabi, S., Khodadadi, A., Mousavi, S.M., Dadashova, B., Lord, D., 2021. Quantifying the automated vehicle safety performance: A scoping review of the literature, evaluation of methods, and directions for future research. Accident Analysis & Prevention 152, 106003. doi:10.1016/j.aap.2021.106003.
- Sun, C., Shrivastava, A., Singh, S., Gupta, A., 2017. Revisiting unreasonable effectiveness of data in deep learning era, in: 2017 IEEE International Conference on Computer Vision (ICCV), pp. 843–852.

- doi:[10.1109/ICCV.2017.97](https://doi.org/10.1109/ICCV.2017.97).
- Sun, J., Zhang, H., Zhou, H., Yu, R., Tian, Y., 2022a. Scenario-based test automation for highly automated vehicles: A review and paving the way for systematic safety assurance. *IEEE Transactions on Intelligent Transportation Systems* 23, 14088–14103. doi:[10.1109/TITS.2021.3136353](https://doi.org/10.1109/TITS.2021.3136353).
- Sun, J., Zhou, H., Xi, H., Zhang, H., Tian, Y., 2022b. Adaptive design of experiments for safety evaluation of automated vehicles. *IEEE Transactions on Intelligent Transportation Systems* 23, 14497–14508. doi:[10.1109/TITS.2021.3130040](https://doi.org/10.1109/TITS.2021.3130040).
- UN ECE R157, 2021. UN Regulation No. 157 - Automated Lane Keeping Systems (ALKS). Standard. The United Nations Economic Commission for Europe.
- Wang, C., Storms, K., Zhang, N., Winner, H., 2024. Runtime unknown unsafe scenarios identification for sotif of autonomous vehicles. *Accident Analysis & Prevention* 195, 107410. doi:[10.1016/j.aap.2023.107410](https://doi.org/10.1016/j.aap.2023.107410).
- Wang, C., Xie, Y., Huang, H., Liu, P., 2021. A review of surrogate safety measures and their applications in connected and automated vehicles safety modeling. *Accident Analysis & Prevention* 157, 106157. doi:[10.1016/j.aap.2021.106157](https://doi.org/10.1016/j.aap.2021.106157).
- Wu, J., Xing, X., Xiong, L., Chen, J., 2024a. Accelerated testing and evaluation of autonomous vehicles based on dual surrogates. *Automotive Innovation* doi:[10.1007/s42154-023-00279-4](https://doi.org/10.1007/s42154-023-00279-4).
- Wu, X., Chen, J., Xing, X., Sun, J., Tian, Y., Liu, L., Shen, Y., 2024b. Lambda: Covering the multimodal critical scenarios for automated driving systems by search space quantization. doi:[10.48550/arXiv.2412.00517](https://doi.org/10.48550/arXiv.2412.00517), [arXiv:2412.00517](https://arxiv.org/abs/2412.00517).
- Wu, X., Xing, X., Chen, J., Shen, Y., Xiong, L., 2022. Risk assessment method for driving scenarios of autonomous vehicles based on drivable area, in: *2022 IEEE 25th International Conference on Intelligent Transportation Systems (ITSC)*, IEEE, Macau, China. pp. 2206–2213. doi:[10.1109/ITSC55140.2022.9922210](https://doi.org/10.1109/ITSC55140.2022.9922210).
- Yin, Q., Ma, Z., Zhu, X., Fang, X., 2023. Test Concrete Scenarios Extraction of Lane-Changing Scenarios Based on China-FOT Naturalistic Driving Data. *SAE Technical Paper 2023-01-7055*. SAE International. Warrendale, PA. doi:[10.4271/2023-01-7055](https://doi.org/10.4271/2023-01-7055).
- Zhang, H., Sun, J., Tian, Y., 2024. Accelerated safety testing for highly automated vehicles: Application and capability comparison of surrogate models. *IEEE Transactions on Intelligent Vehicles* 9, 2409–2418. doi:[10.1109/TIV.2023.3319158](https://doi.org/10.1109/TIV.2023.3319158).
- Zhang, P., Zhu, B., Zhao, J., Fan, T., Sun, Y., 2023a. Safety evaluation method in multi-logical scenarios for automated vehicles based on naturalistic driving trajectory. *Accident Analysis & Prevention* 180, 106926. doi:[10.1016/j.aap.2022.106926](https://doi.org/10.1016/j.aap.2022.106926).
- Zhang, X., Tao, J., Tan, K., Törngren, M., Sánchez, J.M.G., Ramli, M.R., Tao, X., Gyllenhammar, M., Wotawa, F., Mohan, N., Nica, M., Felbinger, H., 2023b. Finding critical scenarios for automated driving systems: A systematic mapping study. *IEEE Transactions on Software Engineering* 49, 991–1026. doi:[10.1109/TSE.2022.3170122](https://doi.org/10.1109/TSE.2022.3170122).
- Zhao, D., Lam, H., Peng, H., Bao, S., LeBlanc, D.J., Nobukawa, K., Pan, C.S., 2017. Accelerated evaluation of automated vehicles safety in lane-change scenarios based on importance sampling techniques. *IEEE Transactions on Intelligent Transportation Systems* 18, 595–607. doi:[10.1109/TITS.2016.2582208](https://doi.org/10.1109/TITS.2016.2582208).
- Zhu, B., Zhang, P., Zhao, J., Deng, W., 2022. Hazardous scenario enhanced generation for automated vehicle testing based on optimization searching method. *IEEE Transactions on Intelligent Transportation Systems* 23, 7321–7331. doi:[10.1109/TITS.2021.3068784](https://doi.org/10.1109/TITS.2021.3068784).